RSC Advances

ROYAL SOCIETY OF CHEMISTRY

www.rsc.org/advances

RSC Advances

ARTICLE

Fabrication of Silver-decorated Sulfonated Polystyrene Microspheres for Surface-Enhanced Raman Scattering and Antibacterial Applications

Received 00th January 20xx,
Accepted 00th January 20xx

DOI: 10.1039/x0xx00000x

www.rsc.org/

Kai Zhao,‡[a] Jie Zhao,‡[c] Chengjiao Wu,[a] Shengwen Zhang,[c] Ziwei Deng,*[ab] Xiaoxi Hu,[b] Mingli Chen *[d] and Bo Peng*[e]

A facile approach was proposed to decorate silver nanoparticles on sulfonated polystyrene microspheres (denoted as SPS@Ag composite microspheres),in which polyvinylpyrrolidone (PVP) was served both as the reductant and stabilizer.In this approach, first, sulfonated polystyrene (SPS) microspheres were synthesized via the sulfonation of monodisperse polystyrene (PS) microspheres in the concentrated sulfuric acid, which were used as the active template cores. Upon the electrostatic attraction between the negatively charged -SO_3H groups and the positively charged $[Ag(NH_3)_2]^+$ ions, silver precursor-$[Ag(NH_3)_2]^+$ ions were easily adsorbed onto the surfaces of sulfonated polystyrene microspheres. These $[Ag(NH_3)_2]^+$ ions were *in-situ* reducedto metallic Ag nanoparticles andsimultaneously protected by PVP, forming the stable SPS@Ag composite microspheres. During the reaction, neither additional reducing agents nor stabilizers were needed. Moreover, by simply adjusting the concentration of $[Ag(NH_3)_2]^+$ ions,the size of Ag nanoparticles and the surface coverage of SPS with Ag nanoparticles can be easily tailored. Finally, it has been proven that these as-synthesized SPS@Ag composite microspheres were the ideal active substrates for the surface-enhanced Raman spectroscopy (SERS) for the trace detection trace of the antibiotics (*i.e.*, Penicillin G sodium and Chloramphenicol), and showed an enhanced antibacterial activity against both *Escherichia coli* (Gram-negative bacteria) and *Staphylococcus aureus* (Gram-positive bacteria) as well.

Introduction

Recently, the smart design of colloidal composite particles in the presence of noble metallic materials (such as Au, Ag, Pd and Pt) has attracted much attention, due to their unique and tunable properties for various applications in optoelectronics, photonic crystals, catalysis, chemical and biological sensors, and surface-enhanced Raman scattering, and so forth.[1-3] In particular, great efforts have been focused on how to prepare Ag nanoparticles based composite particles, not only from the commercial viewpoints but also mainly because they exhibit the unique optical, electronic and catalytic properties which are markedly different from their bulk counterparts.[4, 5] In order to make a full use of the unique characters of Ag nanoparticles, the stability and activity of the Ag nanoparticles have to be guaranteed. This way, decorating Ag nanoparticles onto the inert, yet stable substrates is a relatively simple and effective strategy.

So far, a variety of synthetic routes, such as surface seeding methods and/or electroless plating, surface functionalization deposition, layer-by-layer (LbL) technology, and self-assembly, have been demonstrated to decorate Ag metallic nanoparticles

[a] *School of Materials Science and Engineering, Shaanxi Normal University, Xi'an, 710062, China. E-mail: zwdeng@snnu.edu.cn; Tel:+86-29-81530804.*
[b] *Guangxi Colleges and Universities Key Laboratory of Beibu Gulf oil and Natural Gas Resource Effective Utilization, Qinzhou University, Qinzhou, 535000, China*
[c] *The Key Laboratory of Food Colloids and Biotechnology, Ministry of Education, School of Chemical and Material Engineering, Jiangnan University, Wuxi 214122 , China.*
[d] *Department of Ultrasound in Medicine, Xinhua Hospital Affiliated to Shanghai Jiaotong University School of Medicine, Shanghai, 200092, China. E-mail: dr_mingli_chen@163.com; Tel: +86-21-25077226.*
[e] *Department of Chemistry, Physical and Theoretical Chemistry Laboratory, University of Oxford, South Parks Road, Oxford OX1 3QZ, United Kingdom. E-mail: pengbo006@gmail.com; Tel: +44-1865285417.*
‡ These two authors contributed equally to this work.

onto substrates (*e.g.*, silica and polystyrene).[6-8] Among these impressive approaches, it is noted that the surface functionalization of dielectric colloidal cores is crucial to successfully fabricate composite particles. For example, one of typical surface functionalization is to use the functional linkers or metals (such as organosilanes,[9] $SnCl_2$,[10] palladium[11] and gold[12, 13]) to grant the surface of the colloidal cores owning a specific interaction with Ag nanoparticles or ions; the other is based on the layer-by-layer (LbL) self-assembly of polyelectrolytes and Ag nanoparticles which are alternatively deposited onto the surfaces of the cores.[1] However, it is worth pointing out that some extra reducing agents (such as hydrazine, KBH_4, sodium citrate or ascorbic acid), reducing solvents (dimethylformamide, polyols), or irradiation sources (γ-ray, ultrasound, ultraviolet or microwave) have been introduced to reduce Ag precursors to zero-valence state in some of these methods.[14-18] Sometimes, these extra chemicals or external influence may exert unpredictable effects on the further reaction or future application in essence, for instance, inducing the system unstable. This way, an additional stabilizer is necessary to maintain the stability of the system, which may be hard to select according to the diversity of the chemicals present in the reaction. Moreover, the stabilizer selected should exert a minor influence on the future use of composite particles. On the other hand, the complicated process may burden the time and commercial consumption and decline the quality of the products from the practical viewpoints. Therefore, developing a facile and feasible approach towards the composite particles with a good uniformity in morphology and materials is still highly desired.

As the substrate, the materials have to be inert and stable during the reaction, which also allows the composite particles stable and active during the usage. Moreover, the ease and versatileness of the surface modification of the core templates is also the other important factor that may massively extend the decoration of the other kinds of nanoparticles with promising properties. Among the frequently used dielectric colloidal spheres, polystyrene microspheres with or without functional groups are ideal as the core materials mainly in the basis of their advantageous features, such as, monodisperse in size and shape, tunable in size, easily copolymerizing with various functional co-monomers, controllable in surface group, inert and stable in polar solvents and the ready availability in large amounts from commercial sources.[19-22]

Moreover, polyvinylpyrrolidone (PVP), because of its high chemical stability, nontoxicity and excellent solubility in many solvents, has been demonstrated as an efficient steric stabilizer or capping agent in the chemical synthesis of polymeric and composite particles in different species by our groups and others.[23-28] Recently, PVP has been proved as a reductant which enables to reduce some metal (e.g. Au, Ag, Pd and Pt) salts to their zero-valence metal state nanoparticles in aqueous media, where the reductive nature of PVP is most likely related to its hydroxyl groups.[3] In this paper, we developed a facile method for the decoration of silver nanoparticles onto sulfonated polystyrene microspheres (denoted as SPS@Ag composite microspheres), during which polyvinylpyrrolidone (PVP) was served both as reductant and stabilizer. In this approach, first, monodisperse polystyrene (PS) microspheres were synthesized via dispersion polymerization in an alcoholic environment. Then, PS microspheres were sulfonated by immersing into the concentrated sulfuric acid, and the result sulfonated polystyrene microspheres can be used as the active template cores. Thanks to the electrostatic attraction between sulfonated PS and $[Ag(NH_3)_2]^+$ ions, the surface of the sulfonated PS was saturated with $[Ag(NH_3)_2]^+$ ions, which were *in-situ* reduced to metallic Ag nanoparticles and protected by PVP. As a result, SPS@Ag composite microspheres were obtained. PVP played as the stabilizer and reductant during the preparation, neither additional reducing agents nor stabilizers were necessary. In addition, the size of the Ag nanoparticles and the surface coverage of the core with Ag nanoparticles can be easily controlled by simply adjusting the concentration of $[Ag(NH_3)_2]^+$ ions added. The obtained SPS@Ag composite microspheres showed a high potential in the trace detection of organic compounds, because the Raman spectroscopies of the antibiotics (Peniciline G sodium and Chloramphenicol) were vastly enhanced with the aid of SPS@Ag composite microsphere based substrates. This would be useful for the pesticide and antibiotic residue detection in food industry. Besides that, SPS@Ag composite microspheres were also an ideal candidate in the antibacterial application because of their extraordinary antibacterial performance against *Escherichia coli* (Gram-negative bacteria) and *Staphylococcus aureus* (Gram-positive bacteria).

Experimentalsection

Materials

2, 2'-azobisisobutyronitrile (AIBN) provided by Shanghai Chemical Reagent Co., Ltd. (China) was purified via recrystallization in ethanol prior to use. Styrene (St) was purchased from Tianjin Tianli Chemical Reagent Co., Ltd. (China) and was distilled to remove the inhibitor in vacuum and stored at 4°C until use. Polyvinylpyrrolidone (PVP, MW=40,000 g/mol) was purchased from Sigma-Aldrich and used as received. Silver nitrate ($AgNO_3$, ≥99.8%), aqueous ammonia (28 wt% aqueous solution), sulfuric acid (H_2SO_4, 98%), absolute ethanol were purchased from Sinopharm Chemical Reagent Co., Ltd (China) and used without further purification. Penicillin G sodium and Chloramphenicol were bought from Aladdin Industrial Corporation (China). Ultrapure water (>17MΩcm^{-1}) obtained from a GZY-P10 water system was used throughout the experiments.

Preparation of monodisperse sulfonated polystyrene microspheres

Monodisperse polystyrene (PS) microspheres were used as the templates for the synthesis of sulfonated polystyrene (SPS) microspheres, which were prepared via dispersion polymerization according to our previous work.[25] In detail, first, styrene (20.0 g), PVP (1.8 g), AIBN (0.2 g), ethanol (60.4 g) and water (7.6 g) were added into a 250 mL four-necked round-bottomed flask equipped with a mechanical stirrer, a thermometer with a temperature controller, a N_2 inlet, an Allihn condenser and a heating mantle. After deoxygenating the reaction solution by bubbling nitrogen at room temperature for ca. 1h, the reaction solution was heated up to 70 °C and dispersion polymerization was carried out for 24 h under a constant stirring at a rate of 100 rpm. After the reaction complete, the dispersion was centrifuged and rinsed with ethanol three times. Finally, monodisperse polystyrene (PS) microspheres were dried in a vacuum oven at room temperature for 24 h and stored in air for further use.

Monodisperse sulfonated polystyrene (SPS) microspheres were prepared by sulfonating as-synthesized PS microspheres in the concentrated sulfuric acid.[19] It was described as follows: first, all PS powder (3.0 g) was dispersed into the concentrated sulfuric acid (98%, 30 mL) by sonication. The sulfonation was carried out at 40 °C under a constant stirring at 100 rpm. After 4 h, monodisperse sulfonated polystyrene microspheres were obtained, which were separated by centrifugation, and washed with a large amount of ethanol several times. Ultimately, monodisperse sulfonated polystyrene microspheres were dried in a vacuum oven at room temperature for 24 h and stored in the glass vials for further characterization and experiments.

Fabrication of SPS@Ag composite microspheres

The typical strategy for the decoration of silver nanoparticles onto sulfonated polystyrene microspheres is illustrated in Scheme 1.

The process was described as follows: first, the stock solution was prepared by the dispersion of sulfonated polystyrene microspheres (0.3 g) in ethanol (15 g). Meanwhile, the PVP solution was prepared by dissolving PVP (0.1 g) in ethanol (4 g) at room temperature, which was then mixed with the as-prepared SPS dispersion. Subsequently, 1 mL of freshly prepared $[Ag(NH_3)_2]^+$ ion (0.29 to 1.16 M) aqueous solution was quickly added into the dispersion aforementioned. The mixture was magnetically stirred at room temperature for 1 h. After that, the temperature was elevated to 70 °C and maintained for 7 h under a magnetic stir. The SPS@Ag nanocomposite spheres were collected by centrifugation, and washed with an excess amount of ultrapure water and ethanol several times. In the end, these composite spheres were stored in ethanol for further characterization and experiments.

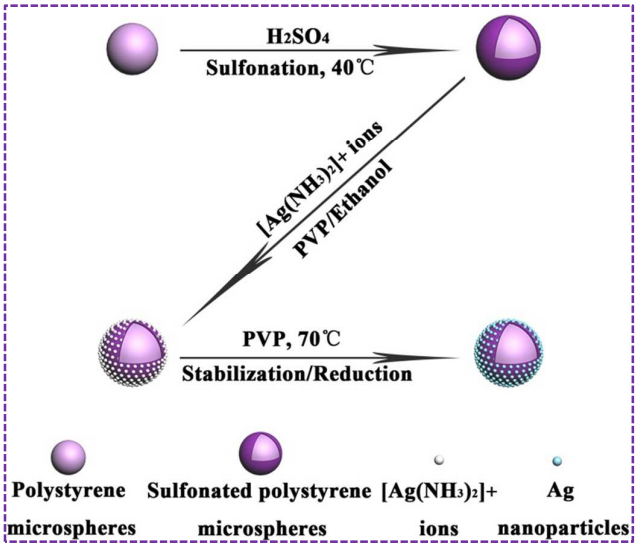

Scheme 1. Schematic diagram illustrating the formation of SPS@Ag composite microspheres prepared by using PVP as the reductant and stabilizer.

SERS measurement

For the SERS measurement, all glass slides were cleaned with

ethanol in an ultrasonic bath for 20 minutes, washed thoroughly with ultrapure water afterwards, and finally, airily dried. The as-prepared SPS@Ag composite microspheres were first dispersed in ethanol, and followed with the deposition of their alcoholic dispersion onto the clean glass slides to form SERS-active substrates. After that, various concentrations of Penicillin G sodium (1×10^{-2} to 1×10^{-10} M) and Chloramphenicol aqueous solutions (1×10^{-3} to 1×10^{-10} M) were dropped onto the SERS-active substrates, respectively. All the Raman measurements were performed at 25 ^{o}C on an inVia Raman Microscope equipped with a 532 nm He-Ne laser. 1mW of laser irradiation intensity was used to excite the samples throughout the experiments. The data acquisition time was 10s for one accumulation. To obtain the reproducible SERS data, all the SERS measurement were carried out under the same conditions iteratively: *e.g.*, each sample was measured 3 times within 10 mins, with 6 randomly chosen areas on the sample, which was focused for 10 s at 25 ^{o}C.

Bacterial culture

In this experiment, two bacterial species-*Escherichia coli* (ATCC 25922) and *Staphylococcus aureus* (ATCC 29213) were selected as the Gram-negative and Gram-positive model bacteria, respectively. For the bacterial culture, the bacterial suspensions were prepared by firstly taking a single colony from the stock bacterial cultures with a loop, and then inoculating in the 5 mL sterile nutrient broth media. After 12 h of incubation in a constant temperature vibrator at 37 ^{o}C with a speed of 200 rpm, both bacterial species at the exponential growth phase were harvested via centrifugation.

Antibacterial assays

In the antibacterial activity assays, the antibacterial test was conducted by the usage of standard disc diffusion assay according to the previous reports on Luria-Bertani (LB) agar medium.[29, 30] In this process, *Escherichia coli* (ATCC 25922) and *Staphylococcus aureus* (ATCC 29213) were used as the experiment strains. Luria−Bertani (LB) medium was used for the bacterial growth. All disks and materials were sterilized in an autoclave prior to the experiments. The disk diffusion assay was performed by placing a 6 mm disk saturated with 1mg/mL of different SPS@Ag dispersions onto an agar plate seeded with *Escherichia coli* and *Staphylococcus aureus*. After 24 h incubation at 37 ^{o}C, the diameters of inhibition zones were measured. The inhibition zones with a bigger diameter indicated a better antibacterial property.

For the kinetic test, *Escherichia coli* and *Staphylococcus aurous*suspensions were inoculated in the LB liquid media containing SPS@Ag composite microspheres at different concentrations (5, 10, 20 and 40 μg/mL for *Escherichia coli* and *Staphylococcus aureus*, respectively). All suspensions were shaken with a shaker at 200 rpm under 37 ^{o}C. The bacterial inhibition growth curves were expressed by the measurement of the optical density (O.D.) of nutrient broth in both media at a wavelength of 600 nm from 0 to 15 h with an interval of 1 h. Similarly, the bacterial suspensions in which only LB liquid medium, and pure SPS microspheres in LB liquid medium (40 μg/mL in both of *Escherichia coli* and *Staphylococcus aureus* samples) were present were selected as the control groups. To better expose the performance of all groups in the antibacterial kinetic tests, the characterizations have been carried out for three times.

Characterization

TEM observation The morphologies of the obtained microspheres (PS, SPS and SPS@Ag composite microspheres) were examined with a transmission electron microscope (TEM, JEOL JEM-2100, Japan). Prior to characterization, all dispersions were diluted with ethanol, and ultrasonically treated at 25 ^{o}C several minutes. Subsequently, samples were dried onto the carbon-coated copper grids ready for the characterization. The average diameters of the microspheres were obtained based on the measurement of more than 100 microspheres in TEM images. The polydispersity (*PD*) was calculated as follows:[24]

$$\overline{D} = \frac{\sum_{i=1}^{N} D_i}{N} \quad (1)$$

$$\sigma = \sqrt{\frac{\sum_{i=1}^{N} (D_i - \overline{D})^2}{N}} \quad (2)$$

$$PD = \frac{\sigma}{\overline{D}} \quad (3)$$

where $\overline{D}$ represents the number-average diameter of the particles, N the number of the particles, and N_i the number of the particle has diameter D_i, respectively. *PD* is calculated based on the standard deviation (σ) and $\overline{D}$ of the system.

FTIR Measurement Fourier-transform infrared spectra of PS microspheres and SPS microspheres were recorded on a Transform Infrared Spectroscope (FTIR, EQUINX55, Brucher Crop, Germany). The sample dispersions were centrifuged and washed with ethanol several times. Subsequently, samples were dried in a vacuum oven for 24 h and pressed into KBr pellets for the FTIR detection.

X-ray photoelectron spectroscopy An AXIS Ultra X-ray photoelectron spectrometer (Kratos Analytical Ltd. U.K.) equipped with a monochromatized Al Kα X-ray source (1486.6 eV) was used to perform the X-ray photoelectron spectroscopy (XPS) measurement. All binding energies were calibrated by using the containment carbon (C1s = 284.6 eV).

X-ray diffraction Powder X-ray diffraction was characterized on a DX-2700 X-ray diffractometer equipped with a Cu tube and a diffracted beam curved graphite monochromator, operating at 40 kV and 30 mA. The crystal structure identification was performed by scanning though the sample powder with a scanning rate of 0.02 degrees (2θ) per second in the range between 10 and 90° (2θ).

TG analysis Thermogravimetric analysis (TGA) was performed on the SDT Q600 (TA Instruments. U.S.A.). All powder samples (PS microspheres, SPS microspheres and SPS@Ag composite microspheres) were heated from 20 to 600 ^{o}C at a rate of 10 ^{o}C/min in the presence of a nitrogen flow at a rate of 50 mL/min.

SERS Measurement Surface-enhanced Raman spectroscopy (SERS) spectra of Penicillin G sodium and Chloramphenicol aqueous solutions adsorbed on the SPS@Ag based SERS-active substrates were recorded on an inVia Raman Microscope (Renishaw, UK) equipped with a 532 nm He-Ne laser. About 1mW of laser irradiation was used to excite the samples. The signal collection time was 10 s.

Results and discussion

Preparation and characterization of monodisperse sulfonated polystyrene microspheres

During last decade, monodisperse polystyrene (PS) microspheres have been widely used as the active templates for the fabrication of composites or hollow spheres at a commercial scale, due to their easy control over the size, yield and surface chemical character.[19, 31-33] For example, negative charged polystyrene microspheres can be obtained by etching their surface with sulfuric acid. The sulfonation of the surface is homogeneous and the spherical shape can be retained. Here, monodisperse homemade polystyrene microspheres were prepared via dispersion polymerization in a single step,[19] which were served as the starters. Immersing into the concentrated sulfuric acid at an elevated temperature (40^{o}C) allows the surface of polystyrene microspheres sulfonated with a negative charge in nature, as illustrated in Scheme 1.

As shown in Fig.1a, the TEM micrograph confirmed that the original PS microspheres prepared via dispersion polymerization were smooth and uniform in size and spherical shape at a large scale with an average diameter of 1.477 μm and a polydispersity of 1.4% (see Fig. 1c). Thus, these monodisperse PS microspheres were ideally as the starters for the following experiments. After the sulfonation, the morphology of the SPS microspheres was also imaged by TEM (Fig. 1b). The size of the SPS microspheres observed was declined to 1.460 μm, while their polydispersity was retained of 2.1% (see Fig. 1d), which clearly indicates that the sulfonation did not have a significant influence on the spherical shape and the size of the PS microspheres because sulfonation reaction slowly occurs homogeneously at the surfaces of PS microspheres. However, compared with the sharp contrast between the original PS particles and the background, the fuzzy edge of the PS microsphere after sulfonation hints the variation of surface chemical composition taking place, although which have to be further proved in aid of other characterization manners.

Therefore, XPS was employed to analyze the surface chemical composition of the PS microspheres and SPS microspheres. As shown in Fig. 1e, before the sulfonation, the strong carbon (C1s) signal peak accompanying with the weak characteristic signals of oxygen (O1s) and nitrogen (N1s) peaks were observed in the XPS scan data of original PS microspheres. The appearance of O1s and N1s peaks with low intensities were attributed to those 'auxiliary' agents, such as AIBN initiator and PVP stabilizer introduced during the dispersion polymerization. After the sulfonation, the C1s, N1s and O1s patterns remained, but the intensity of O1s were greatly enhanced. In addition, the two new signal peaks which were identified as S2s and S2p characteristic patterns, as shown in Fig. 1f, which partially indicated the appearance of -SO_3H groups.

To determine the chemical composition variation, FTIR spectrum is the other powerful tool. Before the sulfonation, the typical polystyrene absorption bands at around 698, 757, 1451, 1493, 1601, 2849, 2923 and 3026 cm^{-1} were clearly shown in the FTIR spectrum of original PS microspheres (spectrum a in Fig. 2). While after the sulfonation occurred, a new absorbance band at 1177 cm^{-1} appeared, which was ascribed to the asymmetric vibration of -SO_3H groups (spectrum b in Fig. 2).[19] In all, combining with the results from TEM and XPS, the successful decoration of -SO_3H group onto PS microspheres can be concluded. In this way, these monodisperse sulfonated PS microspheres can be served as the active templates to prepare composite particles with different shell compositions.[19, 31, 32]

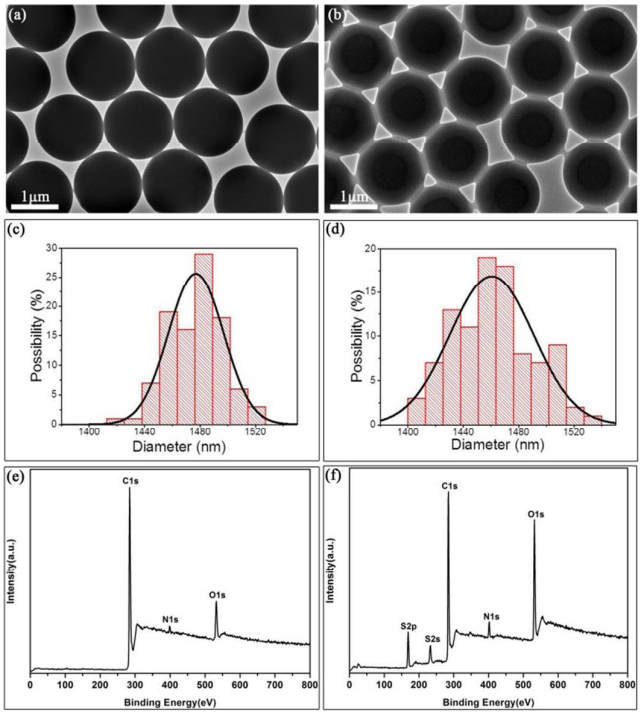

Fig.1(a and b)Transmission electron microscopy (TEM) images and (c and d) the corresponding size distribution histograms and their theoretic fittings of (a) original PS microspheres and (b) SPS microspheres, respectively. X-ray photoelectron spectroscopy (XPS) scans of (e) original PS microspheres in (a) and (f) SPS microspheres in (b).

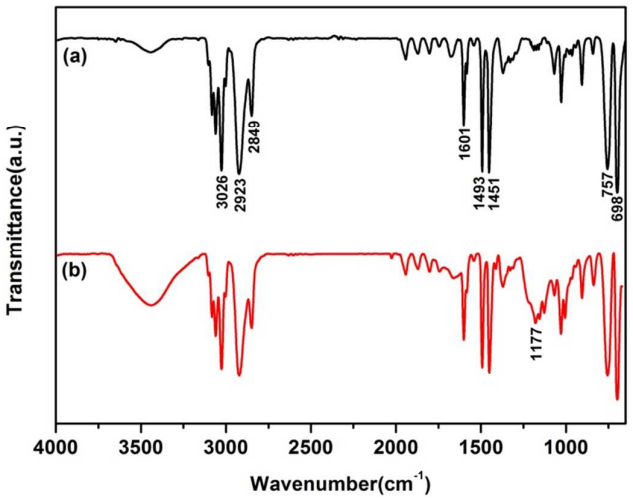

Fig.2 Fourier-transform IR (FTIR) spectra of original PS microspheres (spectrum a) and SPS microspheres (spectrum b).

Preparation and characterization of SPS@Ag composite microspheres

The detailed preparation process of SPS@Ag composite microspheres has been illustrated in Scheme 1. In this approach, the as-prepared monodisperse SPS microspheres served as the active templates were first dispersed into a PVP/ethanol solution. Subsequently, a fresh $[Ag(NH_3)_2]^+$ aqueous solution was added into the SPS microspheres dispersion. $[Ag(NH_3)_2]^+$ ions were easily adsorbed onto the surfaces of the SPS microspheres due to the electrostatic attraction between $-SO_3H$ groups and $[Ag(NH_3)_2]^+$ ions. In this reaction, PVP played two important roles. During the introduction of $[Ag(NH_3)_2]^+$ ions, PVP served as the steric stabilizer enabled to protect SPS microspheres against aggregation. (If PVP were absent, aggregations would be observed in the dispersion because of the rapid neutralization between those negatively charged $-SO_3H$ groups and positive charged $[Ag(NH_3)_2]^+$ ions). When the dispersion was heated to 70 ^oC, the stabilizer role of PVP maintained, while the other role as reductant emerged. During 7 h, $[Ag(NH_3)_2]^+$ ions could be *in-situ* reduced to Ag nanoparticles by PVP, and fixed at the surface of the SPS microspheres. These initially-generated Ag nanoparticles were served as the seeds for the subsequent particle growth. As a result, the relatively big Ag nanoparticles or the complete Ag shells were achieved. [34]

Fig.3 displays the TEM images of SPS@Ag composite microspheres prepared by PVP in ethanol media. In comparison with the template SPS microspheres (see Fig. 1b), the obtained SPS@Ag composite microspheres showed the relative rough surfaces due to the introduction of Ag nanoparticles. From the TEM images, a high contrast between the core and shell materials can be observed, which is a strong evident showing that Ag nanoparticles have been successfully deposited on the template SPS microspheres. When the concentration of $[Ag(NH_3)_2]^+$ ions employed was low, for example, 0.29 M, only a small amount of separate Ag nanoparticles sparsely deposited on the surfaces of template SPS microspheres (see Fig. 3a and b). As the concentration of $[Ag(NH_3)_2]^+$ ions increased from 0.58 to 0.87 M, the amount of Ag nanoparticles loaded on the surfaces of SPS microspheres gradually increased (see Fig. 3d and e, g and h). While further increasing the concentration of $[Ag(NH_3)_2]^+$ ions to1.16M, the composite microspheres with a dense Ag coating were obtained, as shown in Fig.3j. A close inspection of single composite particle from Fig.3j, Ag nanoparticles tended to coalescence to form big Ag cluster because of the high population density of Ag nanoparticles presented on the surface of the SPS

microspheres, as shown in Fig. 3k. To quantitatively demonstrate the size variation of Ag nanoparticles, equations 1, 2 and 3 were used to calculate the size change. As the concentrations of $[Ag(NH_3)_2]^+$ ions were increased from 0.29 to 1.16 M, the average sizes of Ag nanoparticles on the SPS@Ag composite microspheres increased from 16.6 to 21.7 nm, respectively. While the PDI was firstly decreased from 17.3 to 13.6 and to 11.3, then the increased to 23.8%, corresponding to the concentration of $[Ag(NH_3)_2]^+$ ions of 0.29, to 0.58, 0.87 and 1.67 were used, respectively. Initially, the increase in the Ag precursor content resulted in the size growth of the Ag nanoparticles obtained (see Fig. 3c, f and i). While the further increasing the Ag precursor content would lead to the mergence of the Ag nanoparticles, as a result, polydisperse Ag nanoparticles were formed (see Fig. 3l). In summary, these results demonstrate that the particle size and the coverage degree of Ag nanoparticles on the SPS microspheres can be easily tuned by altering the concentration of the silver precursor-$[Ag(NH_3)_2]^+$ ions. In addition, with the protection of PVP, there was no visible aggregation observed.

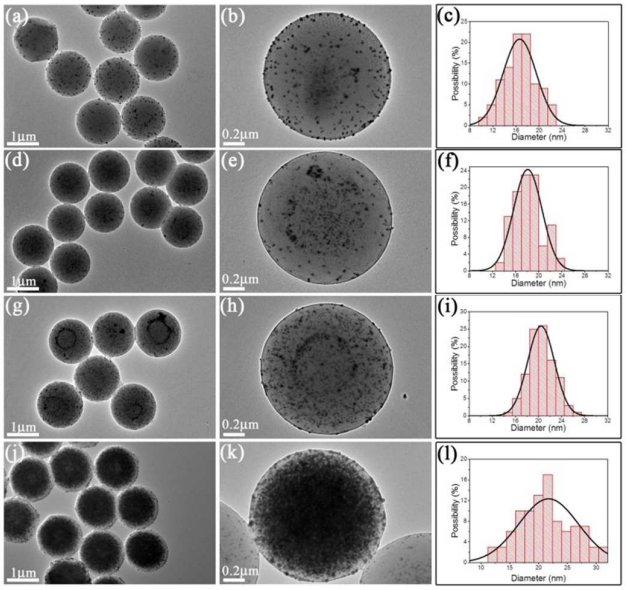

Fig. 3 Transmission electron microscopy (TEM) images of SPS@Ag composite microspheres prepared by using various concentrations of $[Ag(NH_3)_2]^+$ ions: (a and b) 0.29 M; (d and e) 0.58 M; (g and h) 0.87 M; (j and k) 1.16 M. The high magnification TEM images in (b), (e), (h) and (k) show one typical SPS@Ag composite microsphere from (a), (d), (g) and (j), respectively. (c, f, i and l) Their related size distribution histograms and corresponding size fitting of Ag nanoparticles on SPS@Ag composite microspheres.

Similarly, the surface chemical composition of SPS@Ag composite microspheres was also examined by XPS (Fig. 4). Comparing with the XPS spectrum of SPS microspheres in Fig.1f, except S2p, S2s, C1s, N1s and O1s, the new signal peaks including Ag3d ($Ag3d_{5/2}$, $Ag3d_{3/2}$) and Ag3p ($Ag3p_{5/2}$, $Ag3p_{3/2}$) emerged in the XPS spectrum of SPS@Ag composite microspheres in Fig. 4a. These demonstrate the emergence of the silver element in the SPS@Ag composite microspheres. Moreover, a close inspection of Ag 3d peaks in Fig. 4a at around 370 eV showed two individual peaks, as shown in Fig. 4b. The two peaks at 368.6 eV and 374.6 eV with a spin-orbit separation of 6.0 eV correspond to the binding energies of $Ag3d_{5/2}$ and $Ag3d_{3/2}$, respectively. The two characteristic peaks ($Ag3d_{5/2}$ (368.6 eV) and $Ag3d_{3/2}$ (374.6 eV)) further provide the valid evidence to the formation of metallic silver in the system.

X-ray diffraction (XRD) was employed to ascertain the crystal structure of the Ag nanoparticles coated on the SPS@Ag composite microspheres. As shown in Fig. 5a, there is a broad reflection peak present at *2θ* angles between 10 and 30, which is attributed to the amorphous SPS microspheres. While, after the decoration of Ag nanoparticles, the new peaks appear at *2θ* angles of 37.9°, 44.1°, 64.3° and 77.2°, which correspond to the reflections of (111), (200), (220) and (311) crystalline planes of *fcc* structured Ag (JCPDS No.04-0783), respectively (see Fig. 5b).These results indicate that Ag nanoparticles with *fcc* crystal structure can be obtained by the reduction of $[Ag(NH_3)_2]^+$ ions with PVP, which may be applicable to other system where PVP was used as the reductant for $[Ag(NH_3)_2]^+$ ions.[34]

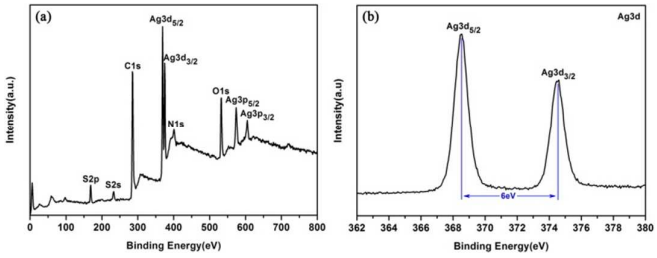

Fig.4 X-ray photoelectron spectroscopy (XPS) scans of (a) SPS@Ag composite microspheres and (b) Ag 3d core–level spectrum of SPS@Ag composite microspheres. SPS microspheres: 0.3 g; PVP: 0.1 g; $[Ag(NH_3)_2]^+$ ions:1.16 M.

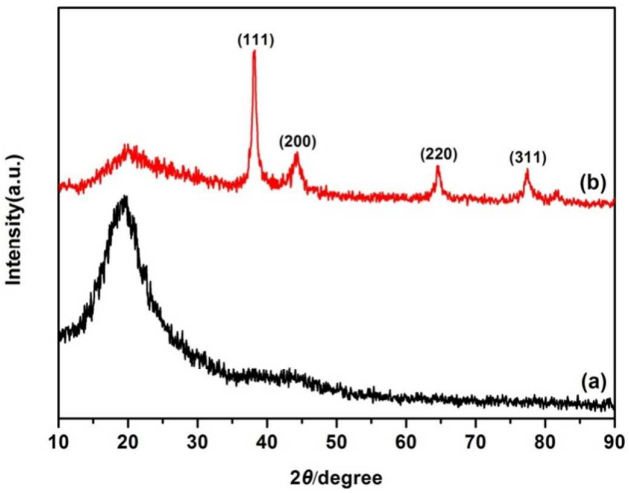

Fig. 5 X-ray diffraction (XRD) patterns of (a) SPS microspheres and (b) SPS@Ag composite microspheres. SPS microspheres: 0.3 g; PVP: 0.1 g; $[Ag(NH_3)_2]^+$ ions: 1.16 M.

In addition, the thermal stability of various as-synthesized particles (PS microspheres, SPS microspheres and SPS@Ag composite microspheres) has been studied by thermogravimetric analysis (TGA). As shown in Fig. 6, the TGA curve of PS microspheres (see Fig. 6a) illustrates that the pure PS microspheres started to lost weight at around 300 ^oC, and ended up to 430 ^oC. It suggests that the decomposition of PS microspheres mainly takes place in the temperature range of 300-430 ^oC. After the sulfonation, the obtained SPS microspheres shows a similar weight loss trend to that of PS microsphere, although it reported that SPS showed a decrease in thermal stability in comparison with pure polystyrene. After the calcination at 600^oC, there are still some inorganic residues preserving in the SPS microspheres (see Fig. 6b).[35]On the other hand, the introduction of Ag nanoparticles on SPS microspheres weighs the final residues after calcination (see Fig. 6c-f).As discussed previously, the surface coverage of the Ag nanoparticles on the SPS microspheres increases with the incremental content of the $[Ag(NH_3)_2]^+$ ions were used. A similar conclusion can also be obtained as reflected from the TGA results, the higher $[Ag(NH_3)_2]^+$ ion concentration was used, the more residue was left over after sintering. As clearly shown in Fig.6c-f, with increasing the concentration of $[Ag(NH_3)_2]^+$ ions from 0.29 M, 0.58 M, 0.87 M to 1.16 M, the final residue weight ratio are increased from 7.9%, 11.9%, 11.7% to 32.1%, respectively, also demonstrating that more Ag nanoparticles were decorated onto SPS@Ag composite microspheres.

Combined all results from TEM, XPS, XRD, FTIR and TGA, the successful preparation of SPS@Ag composite microspheres can be concluded. This approach is simple because neither additional reductant nor stabilizer was utilized during this synthesis process. In addition, the content and the size of Ag nanoparticles loaded can be easily tuned via adjusting the concentration of Ag precursor-$[Ag(NH_3)_2]^+$ ions.

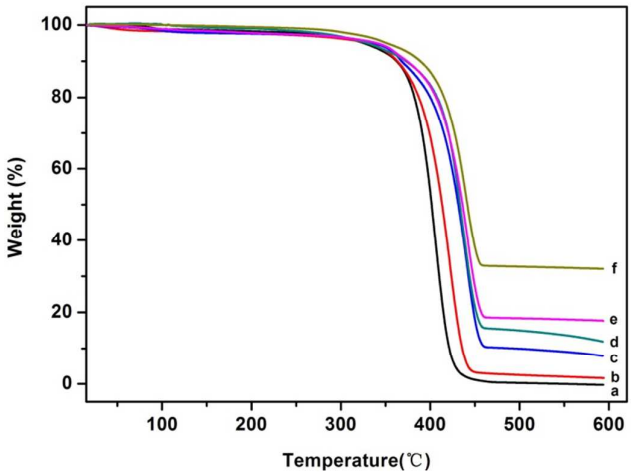

Fig.6 Thermogravimetric analysis (TGA) curves of (a) PS micro spheres, (b)SPS microspheres and (c–f) SPS@Ag composite microspheres prepared by using various concentrations of $[Ag(NH_3)_2]^+$ ions:(c) 0.29 M; (d) 0.58 M; (e) 0.87 M and (f)1.16 M.

SERS Property of SPS@Ag composite microspheres

Commercial antibiotics (e.g. Chloramphenicol, Cephalosporin, Kanamycin, and Penicillin) have been widely used in the clinical treatment of various infectious diseases, which indeed saved a large number of human lives as well as animals. Although some of them have been proved with severely adverse effects when they are overloaded by live entities, they are still used as the clinical medicine, veterinary medicine and feed additive because of their high antibacterial efficiency and low cost. Currently, the abuse and irregularity in the use of antibiotics are often causing the drug residues in animal foods and animal body themselves as well, which will bring the potential health risks to human beings and the ecological environment as well. Therefore, it is eagerly desired to develop a sensitive, reliable and simple method for the detection of the antibiotics.

Raman scattering has been considered as a sensitive and powerful analytical technique for the detection and identification of molecules,

especially, the signals of which will be vastly enhanced when the molecules are adsorbed on the surfaces of plasmonic nanostrcutured materials (This is so-called surface-enhanced Raman scattering, SERS). It has been demonstrated that the significant enhancement is attributed to the highly concentrated electromagnetic fields associated with the strong localized surface plasmonic resonances at the interstitial sites (so-called SERS "hot spots") in those nanostructures consisting of two or more coupled plasmonic metal (e.g., Au or Ag) nanoparticles or nanostrcutured surfaces with closely spaced features.[36, 37] Here, by making use of these as-synthesized SPS@Ag composite microspheres as the "hot spots", the effectively SERS-active substrates can be prepared for the trace detection of the antibiotics. To evaluate the SERS performances of as-synthesized SPS@Ag based substrates, two kinds of antibiotics-Penicillin G sodium and Chloramphenicol were selected as the model probe molecules, separately.

In detail, SPS@Ag composite microspheres with the most Ag loading content (the sample as shown in Fig. 3j) were used to prepare the efficient SERS-active substrates, and followed with the investigation of the SERS trace detection of Penicillin G sodium and Chloramphenicol, respectively. As shown in Fig.7, the corresponding SERS spectra measured at different concentrations of Penicillin G sodium and Chloramphenicol were obtained. For the sake of comparison, the spectra of two antibiotics-Penicillin G sodium and Chloramphenicol deposited on the glass slides in the absence of SPS@Ag composite microspheres were also scanned and shown in Fig. 7a-10 and b-10, respectively. Without the help of SERS active substrate, it was found that no Raman peak was identified at 1×10^{-2} M of Penicillin G sodium (see Fig. 7a-10). But the Raman signals of Penicillin G sodium at 1×10^{-2} M were dramatically magnified in the presence of SPS@Ag composite microspheres, as shown in Fig.7a-1. The main Raman peaks are assigned to the out-of-plane deformation vibrations of beta-lactam and thiazolidine rings (680.2 cm^{-1}), the deformation vibrations of the CH groups from beta-lactam and thiazolidine rings (1378.3 cm^{-1}), the stretching vibration of C-O in the carboxyl (1593.7 cm^{-1}), and the asymmetric stretching vibration of the -CH groups from beta-lactam ring (2939.7cm^{-1}), respectively.[38] To test the sensitivity of the SERS measurement, the concentration of Penicillin G sodium was gradually decreased from 1×10^{-2} to 1×10^{-10} M by a factor of 10^{-1}. As the curves 1-9 shown in Fig. 7a, it was found that the Raman spectral intensities were decreased with less Penicillin G sodium was used. Even when the Penicillin G sodium aqueous solution was diluted to an extreme level as low as 1×10^{-10} M, all characteristic peaks were still distinguishable. To a better view, a locally magnified curve of Fig. 7a-9 was shown in Fig. 7c, in which the signals of SERS were still strong, demonstrating a high sensitivity of this measurement aided by the SERS-active substrate.

To further confirm the high sensitivity also applicable for other antibiotics, the second commercial antibiotic Chloramphenicol was used with the SPS@Ag based SERS-active substrates. Similarly, the Chloramphenicol solution was diluted from 1×10^{-3} to 1×10^{-10} M, and their corresponding SERS spectra were illustrated in Fig. 7b.Three main peaks at 1186.0, 1348.3, 1606.8 cm^{-1}wereattributed to the aromatic C–H in-plane bending, NO_2 symmetric stretching, and ring stretching vibration of chloramphenicol molecule, respectively.[39] In comparison with the curve 1 and 10 in Fig. 7b, it was easily found that the Raman spectral intensities of Chloramphenicol at the concentration of 10^{-3} M were distinctly enhanced in the presence of SERS-active substrates. While, it is hard to distinguish the characteristic patterns of Chloramphenicol at the concentration of 10^{-3} M in the absence of SERS-active substrates (see Fig. 7b-10). Similar to the results of Penicillin G sodium, as the concentration of the Chloramphenicol decreased, the intensity of the peaks was declined. The signals were still detectable when as low as 10^{-10} M of Chloramphenicol was used (see Fig. 7d).

In order to quantitatively study the detection performance, the SERS intensity (*I*) of Penicillin G sodium emerged at 1593.7 cm^{-1} was plotted as a function of Log(C), where C is the concentration of Penicillin G sodium used. As shown in Fig. 7e, the SERS intensity seems linearly increased with increasing the Log ($C_{\text{Penicillin G sodium}}$), which can be fitted in the first order. This fitting may help to roughly determine the concentration limit, lower than which the characteristic patterns of the chemicals would not be detected. For example, if the Penicillin G sodium aqueous solution was diluted to 10^{-11} M, the SERS would not detect Penicillin G sodium anymore. A similar treatment was also carried out with the results of Chloramphenicol in Fig. 7b. As summarized in Fig. 7f, the intensity of Chloramphenicol was decreased with the dilution of Chloramphenicol solution. The concentration limit was observed at 10^{-10} M.

To be easily compared with other reported SERS active materials, the sensitivity of a SERS substrate can be characterized by the enhancement factors (EF) for each given molecule.[34, 40] The SERS enhancement factors (EF) for Penicillin G sodium and Chloramphenicol deposited on the SPS@Ag composite microspheres can be described by:

$$\mathrm{EF} = (I_{SERS} / I_{bulk})(N_{bulk}/N_{ads}) \quad (4)$$

where I_{SERS} and I_{bulk} are the signal intensities of SERS and normal Raman spectra, respectively; N_{bulk} and N_{ads} are the number of molecules in the cross section of the laser beam from the concentrated sample and the number of adsorbed molecules in the cross section of laser beam, respectively. In our experiment, the cross sections of the laser bean were identical for the Raman and SERS performances because the same Raman spectrometer was used. Thus, N_{bulk} and N_{ads} can be replaced by the concentrations of the bulk and SERS samples, respectively.[41, 42] In this experiment, the main Raman bands at 1593.7cm^{-1} and1606.8 cm^{-1} were selected to estimate the EF values for Penicillin G sodium and Chloramphenicol, respectively. Therefore, the EF was calculated to be about 3.16×10^{8} and 3.14×10^{7} for the SERS detection of Penicillin G sodium and Chloramphenicol, respectively, which are higher than the reported results where only nanoparticles were used.[43]

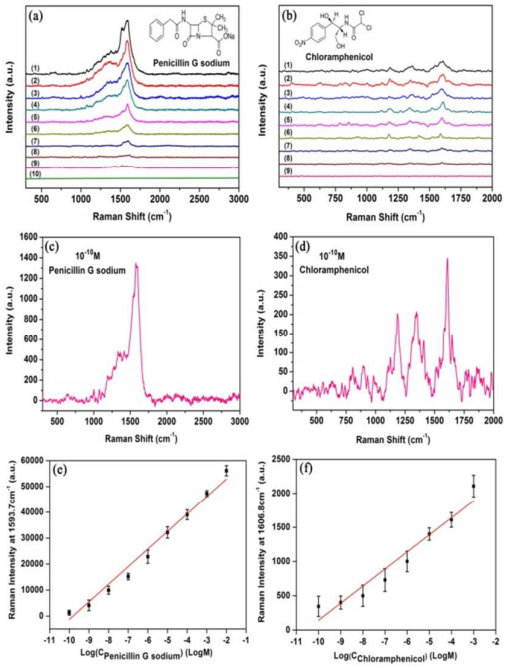

Fig. 7 SERS spectra of (a, c) Penicillin G sodium and (b, d) Chloramphenicol at different concentrations: (a) curves 1-9: 1×10^{-2}-1×10^{-10} M deposited on the SPS@Ag composite microsphere based SERS substrates; curve 10: 1×10^{-2} M, no SPS@Ag composite microspheres were used. (b) curves 1-9: 1×10^{-3}-1×10^{-10} M deposited on the SPS@Ag composite microspheres based SERS substrates; curve 10: 1×10^{-2} M, no SPS@Ag composite microspheres were involved. (c) and (d) The corresponding magnified SERS spectra of Penicillin G sodium at 1×10^{-10} M, Chloramphenicol at 1×10^{-10} M, respectively. (e) and (f) The relationship between SERS intensity at 1593.7 cm^{-1} and 1606.8 cm^{-1} and the concentrations of Penicillin G sodium and Chloramphenicol in aqueous solutions. The coefficients of determination (R^2) are 0.9808 and 0.95579, respectively.

Antibacterial properties of SPS@Ag composite microspheres

Ag nanoparticles and Ag based nanomaterials have been widely employed as the antibacterial materials to fight against infections and control spoilage due to their strong bactericidal activities, broad inhibitory biocidal spectra for many different types of microorganisms including bacteria, fungi and virus, and relatively low toxicities to humans and other animals.[44-47] Concerning the prospective applications of these as-synthesized SPS@Ag composite microspheres as the antibacterial materials, two bacterial species-*Escherichia coli* (Gram-negative bacteria) and *Staphylococcus aureus* (Gram-positive bacteria) were selected to practically evaluate the antibacterial properties of the SPS@Ag composite microspheres in the current work.

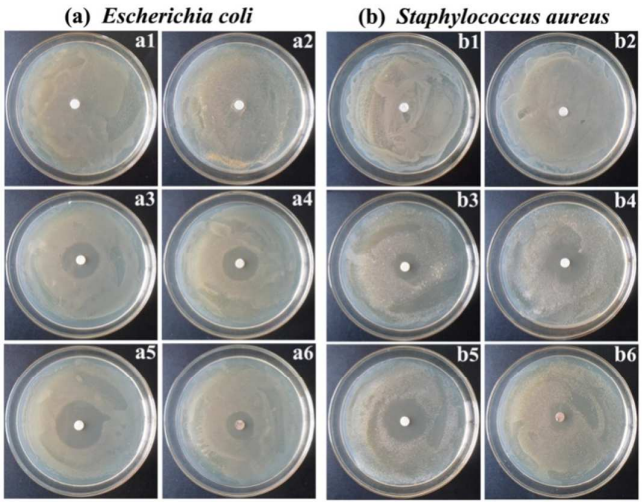

Fig. 8 Comparison of the inhibition zone between (a1 and b1) control groups, the ultrapure water were used as control, (a2 and b2) pure SPS microspheres, 1 mg/mL; and the SPS@Ag composite microspheres (1 mg/mL) prepared by using various concentrations of $[Ag(NH_3)_2]^+$ ions: (a3 and b3) 0.29 M; (a4 and b4) 0.58 M; (a5 and b5) 0.87 M; (a6 and b6) 1.16 M. (a1-a6: for *Escherichia coli*;b1-b6: for *Staphylococcus aureus*).

First, we employed the modified Kirby–Bauer method by measuring the growth inhibition of the bacteria on solid Luria−Bertani (LB) agar plates to investigate the antibacterial activities of SPS@Ag composite microspheres. During the disk diffusion assay, those discs were saturated with different SPS@Ag composite microspheres. For the comparison, the ultrapure water and pure SPS microspheres were also used. Subsequently, all discs were placed on LB agar plates and seeded with *Escherichia coli* and *Staphylococcus aureus*, individually. After the incubation at 37 °C

for 24 h, the antibacterial effects of SPS@Ag composite microspheres against *Escherichia coli* and *Staphylococcus aureus* were evaluated by measuring the size of the inhibition zones on the solid Luria–Bertani (LB) agar plates. As shown in Fig. 8, the inhibition zones surrounding the discs cannot be found in the blank control groups (a1 and b1) and pure SPS microspheres groups (a2 and b2), indicating a bacterial-friendly feature of SPS microspheres with *Escherichia coli* and *Staphylococcus aureus*. On the contrary, when the as-synthesized SPS@Ag composite microspheres were used in the experiment groups, all the bacteria surrounding discs were killed and left distinctly visible zones where no bacterial growth took place (see Fig. 8, a3-a6 and b3-b6).As shown in blank control (see Fig. 8a1 and b1) and pure SPS microsphere groups (see Fig. 8a2 and b2), pure SPS microspheres groups (a2, b2) cannot inhibit both strains of the bacterial growth, which indicates that the antibacterial activities of the SPS@Ag composite microspheres were mainly drawn from the Ag nanoparticles decorated on the surfaces of the SPS microspheres. The details of the inhibition zone diameters for those samples against *Escherichia coli* and *Staphylococcus aureus* have been summarized in Table 1. According to results in Fig. 8 and Table 1, all samples of SPS@Ag composite microspheres indicated good antibacterial activities against *Escherichia coli* and *Staphylococcus aureus*. As the amount of Ag nanoparticles decorated on the SPS microspheres increased, the sizes of the inhibition zone for both *Escherichia coli* and *Staphylococcus aureus* were increased, e.g., the diameters of inhibition zone against *Escherichia coli* increased from 25.0 (Fig. 8a3) to 25.4 (Fig. 8a4) and further to 33.8 mm (Fig. 8a5), when the concentration of $[Ag(NH_3)_2]^+$ ions was increased from 0.29 (sample in Fig. 3a) to 0.58 (Fig. 3d) and further to 0.87 M (Fig. 3g). The similar incremental antibacterial activity was also observed in the *Staphylococcus aureus* groups (see Fig. 8b3-5). However, further increasing $[Ag(NH_3)_2]^+$ ions to 1.16 M only resulted in the merge of Ag nanoparticles into big cluster (see Fig. 3j and k). Correspondingly, the active exposed surface of Ag would be decreased, which only led to an adverse effect on the antibacterial performance. Indeed, as shown in Fig. 8a6 and b6, and Table 1, the diameters of inhibition zones for *Escherichia coli* and *Staphylococcus aureus* were decreased to 23.4 and 18.1 mm, respectively, as the SPS@Ag composite microspheres made from 1.16 M of $[Ag(NH_3)_2]^+$ ions were used as the biocide. Therefore, it is obvious that the antibacterial activity of SPS@Ag composite microspheres will be greatly improved with increasing the amount of individual Ag nanoparticles decorated on the surface of the template SPS microspheres.[48] The larger Ag surface exposed to the environment, the better antibacterial performance will be shown. In addition, the difference in the inhibition zone diameters suggested that SPS@Ag composite microspheres showed the better antibacterial effects against *Escherichia coli* (Gram-negative bacteria) rather than *Staphylococcus aureus* (Gram-positive bacteria), which may be ascribed to the fact that the membranes of the Gram-positive bacteria are thicker and more stable than those of Gram-negative bacteria.[49] Moreover, Gram-positive bacteria generally show less susceptibility to antibacterial agents containing Ag nanoparticles, than Gram-negative bacteria.[50]

We further quantitatively evaluated the antibacterial properties of SPS@Ag composite microspheres by studying their bacteria growth kinetics in the LB liquid media. In this process, SPS@Ag composite microspheres prepared by using 0.87 M of $[Ag(NH_3)_2]^+$ ions was chosen as the model antibacterial agent for the antibacterial investigation. First, the bacteria (*Escherichia coli* and *Staphylococcus aurous*) suspensions were inoculated in the LB liquid media in the presence of various concentrations of SPS@Ag composite microspheres. Then, the bacterial proliferation was monitored by the optical density at 600 nm (O.D. 600) based on the turbidity of the cell suspension within 15 h. The pure SPS microspheres showed a similar tendency with the control groups in both strains. Alternatively, the presence of the SPS@Ag composite microspheres led to a suppressed or completely inhibited growth for both strains. This difference indicates that the antibacterial activity of the SPS@Ag composite microspheres is mainly from the Ag nanoparticles decorated, while the pure SPS did not show an obvious antibacterial activity. The growth curves of the bacteria showed a typical dose-dependent antibacterial effect (see Fig. 9a and b). Compared to the growth curves of the control groups, the bacterial growth in (*Escherichia coli* and *Staphylococcus aureus*) suspensions where the low concentrations (*e.g.*, 5 and 10 μg/mL) of SPS@Ag composite microspheres were present were slightly retarded. As the higher concentration of SPS@Ag composite microspheres was dispersed in the bacteria suspensions, the smaller the bacterial growth rates would be achieved. Remarkably, the growth of the bacteria was completely inhibited during the whole 15 h of culture period when the minimum inhibition concentrations (MIC) of the SPS@Ag composite microspheres (20 μg/mL for *Escherichia coli* and 40 μg/mL for *Staphylococcus aureus*) were used, respectively. A higher concentration than MIC would solely result in the inhibition of the bacterial growth (see the curve of 40 μg/ml in Fig. 9a). The difference of MIC also hints that *Escherichia coli* (Gram-negative

Table 1. The detailed zone diameters of the inhibition zone tests for the SPS@Ag composite microspheres against *Escherichia coli* and *Staphylococcus aureus*

	Initial diameter (mm)		Final inhibition zone diameter(mm)		Diffusion [b] (mm)	
Sample [a]	*Escherichia coli*	*Staphylococcus aureus*	*Escherichia coli*	*Staphylococcus aureus*	*Escherichia coli*	*Staphylococcus aureus*
Ultrapure water	6.0	6.0	6.0	6.0	0.0	0.0
SPS	6.0	6.0	6.0	6.0	0.0	0.0
SPS@Ag-1	6.0	6.0	25.0	18.2	19.0	12.2
SPS@Ag-2	6.0	6.0	25.4	25.1	19.4	19.1
SPS@Ag-3	6.0	6.0	33.8	30.0	27.8	24.0
SPS@Ag-4	6.0	6.0	23.4	18.1	17.4	12.1

[a]: The ultrapure water and pure SPS microspheres (1 mg/mL) were used as the control groups; SPS@Ag composite microspheres (1mg/mL) prepared at the various concentrations of $[Ag(NH_3)_2]^+$ ions (0.29, 0.58, 0.87 and 1.16 M) are denoted as SPS@Ag-1,SPS@Ag-2,SPS@Ag-3 and SPS@Ag-4, respectively, their morphologies were shown in Fig. 3.

[b]: Diffusion (mm) =Final inhibition zone diameter (mm) – Initial diameter (mm)

bacteria) was more sensitive against the SPS@Ag composite microspheres than *Staphylococcus aureus* (Gram-positive bacteria).

As aforementioned, the strong antibacterial activities of these SPS@Ag composite microspheres are probably ascribed to the Ag nanoparticles attached. On the basis of our antibacterial results and the knowledge from literatures,[51-56] their antibacterial activities can be explained by the following possible bactericidal mechanism: (1) These silver-based nanomaterials may directly interact with the sulfur-contained proteins in the cell membrane of the bacteria, which straight causes the structural changes or functional damages to the bacterial cell membrane, and further results in the death of the bacteria;[51, 54] (2) The Ag ions releasing from silver-based materials are able to interact with the disulfide or sulfhydryl groups of the enzymes in the bacteria, causing the structural changes and further destroying the metabolic process of the bacterial cells, all of which can inactivate the microorganism cells and lead to cell deathin the end.[57, 58]

Conclusions

In summary, we presented a facile approach to fabricate SPS@Ag composite microspheres with the aid of PVP served both as the reductant and stabilizer. During the synthesis, neither additional reductants nor stabilizers were necessary. Through a rich variety of characterizations (*e.g.*, TEM, XPS, FTIR, TGA and XRD), the formation and property of the SPS@Ag composite microspheres have been fully investigated. Moreover, the particle size of Ag nanoparticles and the Ag coverage degree on the SPS@Ag composite microspheres could be facilely tailored by adjusting the concentration of the silver precursor-$[Ag(NH_3)_2]^+$ ions. In addition, the preliminary SERS measurements indicated that these as-synthesized SPS@Ag composite microspheres can be used as the ultrasensitive SERS substrates for the trace detection of antibiotics (*i.e.*, Penicillin G sodium and Chloramphenicol), which may be useful for the food testing. On the other hand, in the antibacterial assays, these as-synthesized SPS@Ag composite microspheres exhibited extraordinary antibacterial activities against *Escherichia coli* (Gram-negative bacteria) and *Staphylococcus aureus* (Gram-positive bacteria). Based on these results, we believe these SPS@Ag composite microspheres can be broadly used as the SERS-active substrates for the biomedical and environmental applications and as the promising potential antibacterial materials for future biomedical applications.

Moreover, this approach also presents a versatile paradigm for the preparation of many types of materials with complex shapes. On the basis of this technique, a number of nanocomposite materials coated with a diversity of metallic (Au, Ag, Pd and Pt, etc.) nanoparticles could be achieved, which may show the unique promising feature for biological and materials applications.

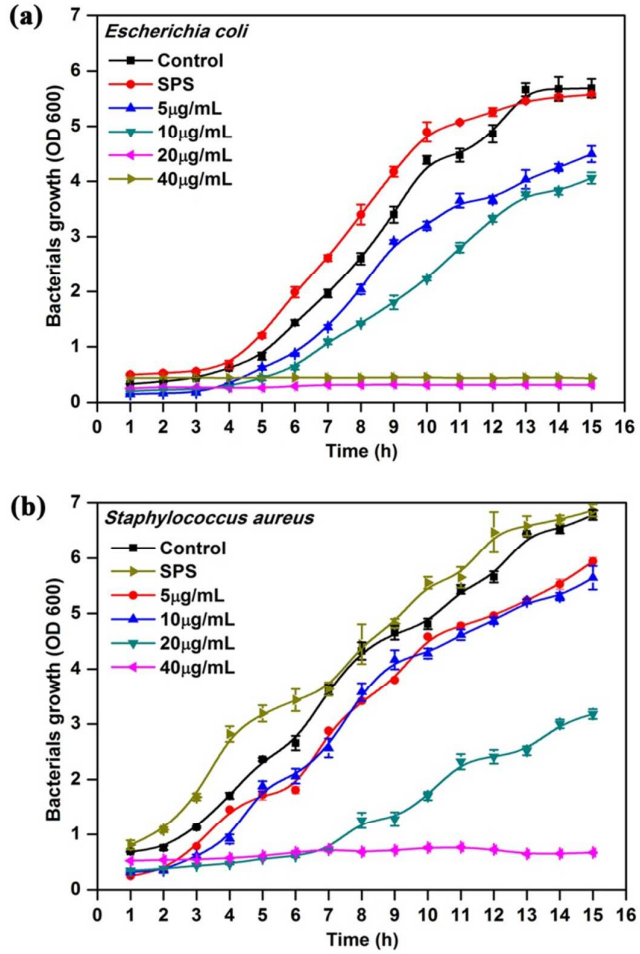

Fig. 9 Bacterial growth curves employed to evaluate the antibacterial activities of the SPS@Ag composite microspheres against (a) *Escherichia coli* and (b) *Staphylococcus aureus*. Pure SPS microspheres and SPS@Ag composite microspheres at different concentrations (5, 10, 20, 40 μg/mL for both *Escherichia coli* and *Staphylococcus aureus*, respectively) were added to the culture of *Escherichia coli* and *Staphylococcus aureus*. LB liquid medium was used in the control experiments. The growth of the bacteria was measured by the judgment of O.D. at a wavelength of 600 nm. The initial addition of the SPS@Ag composite microspheres to the LB bacterium suspension was regarded as the starting point.

Acknowledgements

The financial supports from the National Natural Science Foundation of China (No. 51203087, 51473089), the Natural Science Basic Research Plan in Shaanxi Province of China (No. 2013JQ2006), the Science and Technology Program of Shaanxi Province (No.2015KJXX-20), the Fundamental Research Funds for the Central Universities (No. GK201503039, GK201501002, GK201301002, GK201101003), the Scientific Research Foundation for the Returned Overseas Chinese Scholars, State Education Ministry, the Opening Project of Guangxi Colleges and Universities Key Laboratory of Beibu Gulf oil and Natural Gas Resource Effective Utilization (No.2014KLOG08), the Natural Science Foundation of Guangxi (No.2013GXNSFBA019253) and the Science and Technology Research Project for Universities of Guangxi (No.2013ZD071) for this research are appreciated.

Notes and references

1 T. Cassagneau and F. Caruso, *Adv. Mater.* , 2002, **14**, 732-736.
2 Z. J. Jiang, C. Y. Liu and L. W. Sun, *J. Phys. Chem. B*, 2005, **109**, 1730-1735.
3 Z. W. Deng, M. Chen and L. M. Wu, *J. Phys. Chem. C*, 2007, **111**, 11692-11698.
4 Y. Sun and Y. Xia, *Science*, 2002, **298**, 2176-2179.
5 Y. N. Xia, Y. J. Xiong, B. Lim and S. E. Skrabalak, *Angew. Chem.Int. Ed.*, 2009, **48**, 60-103.
6 X. Peng, J. Chen, J. A. Misewich and S. S. Wong, *Chem. Soc. Rev.*, 2009, **38**, 1076-1098.
7 S. E. Habas, P. D. Yang and T. Mokari, *J. Am. Chem. Soc.*, 2008, **130**, 3294-3295.
8 S. E. Habas, H. Lee, V. Radmilovic, G. A. Somorjai and P. Yang, *Nat. Mater.*, 2007, **6**, 692-697.
9 B. J. Jankiewicz, D. Jamiola, J. Choma and M. Jaroniec, *Adv. Colloid Interface Sci.*, 2012, **170**, 28-47.
10 Y. Kobayashi, V. Salgueirino-Maceira and L. M. Liz-Marzan, *Chem. Mater.*, 2001, **13**, 1630-1633.
11 A.Warshawsky and D. A. Upson, *J.Polym.Sci.PartA: Polym. Chem.*, 1989, **27**, 2963-2994.
12 J. B. Jackson and N. J. Halas, *J. Phys. Chem. B*, 2001, **105**, 2743-2746.
13 S. J. Oldenburg, R. D. Averitt, S. L. Westcott and N. J. Halas, *Chem. Phys. Lett.*, 1998, **288**, 243-247.
14 F. Gao, Q. Lu and S. Komarneni, *Chem. Mater.*, 2005, **17**, 856-860.
15 A. Henglein and M. Giersig, *J. Phys. Chem. B*, 1999, **103**, 9533-9539.
16 H. H. Huang, X. P. Ni, G. L. Loy, C. H. Chew, K. L. Tan, F. C. Loh, J. F. Deng and G. Q. Xu, *Langmuir*, 1996, **12**, 909-912.
17 I. Pastoriza-Santos and L. M. Liz-Marzán, *Langmuir*, 2002, **18**, 2888-2894.

18 A. L. Rogach, G. P. Shevchenko, Z. M. Afanas'ev and V. V. Sviridov, *J. Phys. Chem. B*, 1997, **101**, 8129-8132.
19 Z. W. Deng, M. Chen, G. X. Gu and L. M. Wu, *J. Phys. Chem. B*, 2008, **112**, 16-22.
20 Z. W. Deng, M. Chen, S. X. Zhou, B. You and L. M. Wu, *Langmuir*, 2006, **22**, 6403-6407.
21 Z. W. Deng, Z. P. Zhen, X. X. Hu, S. L. Wu, Z. S. Xu and P. K. Chu, *Biomaterials*, 2011, **32**, 4976-4986.
22 Z. N. Li, C. J. Wu, K. Zhao, B. Peng and Z. W. Deng, *Colloid Surf. A:Physicochem. Eng. Asp.*, 2015, **470**, 80-91.
23 B. Peng, A. van Blaaderen and A. Imhof, *Acs Appl.Mater. Interfaces*, 2013, **5**, 4277-4284.
24 B. Peng, E. van der Wee, A. Imhof and A. van Blaaderen, *Langmuir*, 2012, **28**, 6776-6785.
25 Z. Chen, J. Fu, Q. Xu, Y. Guo, H. Zhang, J. Chen, J. Zhang, G. Tian and B. Yang, *J. Colloid Interface Sci.*, 2013, **391**, 54-59.
26 C. Graf, D. L. J. Vossen, A. Imhof and A. van Blaaderen, *Langmuir*, 2003, **19**, 6693-6700.
27 B. Peng and A. Imhof, *Soft Matter*, 2015, **11**, 3589-3598.
28 B. Peng, H. R. Vutukuri, A. van Blaaderen and A. Imhof, *J. Mater. Chem.*, 2012, **22**, 21893-21900.
29 D. E. Conner and L. R. Beuchat, *J. Food Sci.*, 1984, **49**, 429-434.
30 M. Elgayyar, F. A. Draughon, D. A. Golden and J. R. Mount, *J. Food Prot.*, 2001, **64**, 1019-1024.
31 Z. W. Niu, Z. H. Yang, Z. B. Hu, Y. F. Lu and C. C. Han, *Adv. Funct. Mater.*, 2003, **13**, 949-954.
32 Z. Z. Yang, Z. W. Niu, Y. F. Lu, Z. B. Hu and C. C. Han, *Angew. Chem.Int. Ed.*, 2003, **42**, 1943-1945.
33 M. Chen, L. Hu, J. Xu, M. Liao, L. Wu and X. Fang, *Small*, 2011, **7**, 2449-2453.
34 K. Zhao, C. Wu, Z. Deng, Y. Guo and B. Peng, *RSC Adv.*, 2015, **5**,52726-52736.
35 C. R. Martins, G. Ruggeri and M.A. De Paoli, *J. Braz. Chem. Soc.*, 2003, **14**, 797-802.
36 Y. Lu, Y. Mei, M. Drechsler and M. Ballauff, *Angew. Chem.Int. Ed.*, 2006, **45**, 813-816.
37 Y. Lu, Y. Mei, M. Ballauff and M. Drechsler, *J. Phys. Chem. B*, 2006, **110**, 3930-3937.
38 P. L. Stiles, J. A. Dieringer, N. C. Shah and R. R. Van Duyne, *Annu.Rev.Anal.Chem*, 2008, **1**, 601-626.
39 T. Iliescu, M. Baia and I. Pavel, *J. Raman Spectrosc.*, 2006, **37**, 318-325.
40 D. Sajan, G. D. Sockalingum, M. Manfait, I. Hubert Joe and V. S. Jayakumar, *J. Raman Spectrosc.*, 2008, **39**, 1772-1783.
41 E. C. Le Ru, E. Blackie, M. Meyer and P. G. Etchegoin, *J. Phys. Chem. C*, 2007, **111**, 13794-13803.
42 B. K. Jena, B. K. Mishra and S. Bohidar, *J. Phys. Chem. C*, 2009, **113**, 14753-14758.
43 Y. Liu, L. L. Liu and R. Guo, *Langmuir*, 2010, **26**, 13479-13485.
44 V. K. Sharma, R. A. Yngard and Y. Lin, *Adv. Colloid Interface Sci.*, 2009, **145**, 83-96.
45 C. Marambio-Jones and E. M. V. Hoek, *J. Nanopart. Res.*, 2010, **12**, 1531-1551.
46 S. Chernousova and M. Epple, *Angew. Chem.Int. Ed.*, 2013, **52**, 1636-1653.
47 N. R. Panyala, E. M. Pena-Mendez and J. Havel, *J. Appl. Biomed*, 2008, **6**, 117-129.
48 Y. H. Kim, D. K. Lee, H. G. Cha, C. W. Kim and Y. S. Kang, *J. Phys. Chem. C*, 2007, **111**, 3629-3635.
49 J. Njagi, M. M. Chernov, J. C. Leiter and S. Andreescu, *Anal. Chem.*, 2010, **82**, 989-996.
50 E. Fortunati, S. Mattioli, L. Visai, M. Imbriani, J. L. G. Fierro, J. M. Kenny and I. Armentano, *Biomacromolecules*, 2013, **14**, 626-636.
51 Q. L. Feng, J. Wu, G. Q. Chen, F. Z. Cui, T. N. Kim and J. O. Kim, *J. Biomed. Mater. Res.*, 2000, **52**, 662-668.
52 J. R. Morones, J. L. Elechiguerra, A. Camacho, K. Holt, J. B. Kouri, J. T. Ramirez and M. J. Yacaman, *Nanotechnology*, 2005, **16**, 2346-2353.
53 S. Egger, R. P. Lehmann, M. J. Height, M. J. Loessner and M. Schuppler, *Appl. Environ. Microbiol.*, 2009, **75**, 2973-2976.
54 H. Y. Lee, H. K. Park, Y. M. Lee, K. Kim and S. B. Park, *Chem. Commun.*, 2007, 2959-2961.
55 J. Z. Ma, J. T. Zhang, Z. G. Xiong, Y. Yong and X. S. Zhao, *J. Mater. Chem.*, 2011, **21**, 3350-3352.
56 Z. Zhang, J. Zhang, B. Zhang and J. Tang, *Nanoscale*, 2013, **5**, 118-123.
57 Y. Matsumura, K. Yoshikata, S. Kunisaki and T. Tsuchido, *Appl. Environ. Microbiol.*, 2003, **69**, 4278-4281.
58 A. Gupta, M. Maynes and S. Silver, *Appl. Environ. Microbiol.*, 1998, **64**, 5042-5045.

Table of contents entry

A facile approach was presented to prepare SPS@Ag composite microspheres with surface-enhanced Raman scattering properties and enhanced antibacterial activities.